JOURNAL OF MATERIALS SCIENCE 32 (1997) 4701–4709

Three-dimensional shape of the Y_2BaCuO_5 pattern in melt-textured Y–Ba–Cu–O oxide

CHAN-JOONG KIM, KI-BAIK-KIM, HAI-WOONG PARK, IL-HYUN KUK, GYE-WON HONG
Superconductivity Research Laboratory, Korea Atomic Energy Research Institute, P.O. Box 105, Yusung, Taejon, 305-600, South Korea

Crystallographic orientations of the Y211 tracks that were trapped within the melt-textured Y123 domains were determined from the orientation relationship among the Y211 pattern, $\langle 1\,1\,0 \rangle$ twin traces and a microcrack. Analysing the orientation of the two-dimensional Y211 patterns that were observed on various crystallographic planes of the Y123, the three-dimensional shape of the Y211 pattern was inferred as follows: only one *x*-type Y211 pattern was included within one Y123 domain and three sets of diagonal Y211 tracks met with the corners of the Y123 domain. The diagonal Y211 tracks lie on the (1 1 0), ($\bar{1}$ 1 0), (0 1 1), (0 $\bar{1}$ 1), (1 0 1) and (1 0 $\bar{1}$) planes of the Y123 domain. The planes where the Y211 tracks are located are considered to be the boundary planes where local growing parts of the Y123 domain impinge upon each other. The formation mechanism of the Y211 pattern is discussed on the basis of anisotropic growth behaviour and the shape of the Y123 domain.

1. Introduction

Various melt processing methods [1–7], which are used for fabrication of a Y–Ba–Cu–O superconductor with high critical current density, J_c, consist of complicated heating cycles near the peritectic temperature of the Y–Ba–Cu–O system at which the Y_2BaCuO_5 (Y211) phase reacts with the liquid phase to form the textured $YBa_2Cu_3O_{7-y}$ (Y123) domain. During the peritectic reaction, Y211 inclusions are frequently trapped within the textured Y123 superconducting matrix [1–3], owing to inconsistency between the dissolution rate of the Y211 and the growth rate of the Y123 domains [8, 9]. An interesting feature of Y211 is the fact that the Y211 distribution within Y123 is not uniform [10–14]. Two types of non-uniform distributions of Y211 were observed: spherical Y211 free regions [13] and linear Y211 segregation along specific crystallographic directions of Y123 [10–12]. Several studies [10–13] have shown that the Y211 pattern has an *x*-type shape within the Y123 domain. Up to now, however, the orientation analysis for the Y1211 tracks has been limited on the local two-dimensional crystallographic plane, i.e. the *a–b* plane of the Y123 domain [10, 12]. The three-dimensional shape of the Y211 pattern is still not understood.

Formation of the Y211 pattern was suggested to be related closely to particle (Y211) interaction at the advancing Y123–liquid interface [12]. In our previous work [12] and in another study [15], the trapping behaviour of Y211 during peritectic growth of the Y123 domain was explained by the Uhlmann–Chalmer–Jackson (UCJ) theory [16], which described particle interaction in terms of interfacial energy among particle–solid, solid–liquid and particle–liquid. However, this theory could not explain the reason why the Y211 particles were trapped to form tracks along specific crystallographic orientations of Y123. Because the Y211 tracks are formed during the growth of Y123 domains, evaluation of the orientations of the Y211 tracks will be helpful in understanding the growth mechanism of the melt-processed Y123 domain. Furthermore, this work will be practically important in achieving high critical current [17] and reliable mechanical properties [18] via improvement of the uniformity of the Y211 distribution.

The aim of this study is to construct a three-dimensional shape from the orientation data evaluated from the two-dimensional Y211 tracks. Various Y211 patterns on polished surfaces of the melt-textured Y123 samples are examined and their orientations are determined from the orientation relationship among the Y211 tracks, twin traces and a microcrack. The three-dimensional shape of the Y211 tracks is constructed by combining the various two-dimensional Y211 patterns. The formation mechanism of the Y211 pattern is discussed on the basis of the growth mechanism of the Y123 domain during peritectic reaction.

2. Experimental procedure

2.1. Sample preparation

The Y123 powder used in this experiment was prepared by the conventional solid-state reaction method of Y_2O_3, $BaCO_3$ and CuO powder of 99.9% purity.

0022–2461

The powders were weighed to the cation ratio of Y : Ba : Cu = 1 : 2 : 3, ball-milled in acetone for 20 h and then dried in air. The ball-milled powder was calcined in air at 880 °C for 50 h with repeated crushing every 10 h and then cooled in a furnace after the final heat treatment. The calcined Y123 powder was uniaxially pressed into pellets in a steel die and then isostatically pressed in an oil chamber. The pellets were sintered in air at 950 °C for 10 h and then cooled in air. The sintered pellets were placed on a (0 0 1) MgO single crystal so as to limit the melt loss during partial melting [19] and then conventional melt-texture heat treatment followed. The pellets were heated to 1050–1100 °C in air at a rate of 100 °C h^{-1}, held for 1 h at this temperature, cooled to 1010 °C at a rate of 100 °C h^{-1}, cooled to 970 °C at a rate of 1–5 °C h^{-1}, and then cooled to room temperature at a rate of 100 °C h^{-1}. The melt-textured Y123 pellets were mounted using epoxy resin, ground with SiC paper up to 600 grit and then polished with 1 μm diamond paste. The polished surfaces were etched in 1% HCl solution for 1–5 s and then cleaned in alcohol using an ultrasonic cleaner. The microstructure of the melt-textured Y123 samples was analysed for polished and etched surfaces using optical and scanning electron microscopes (SEM).

2.2. Determination orientation of a polished plane of the Y123

The method of determining the orientation of the polished surface of Y123 grains was well established in the polycrystalline Y123 sample [20]. This technique utilizes the orientation relationship among the two twin traces and the direction of the longer side of the plate-like Y123 grains. In the case of the melt-textured Y123 sample, instead of the longer side of the grain, the direction of the microcrack can be used for orientation evaluation. The orientation of the polished surface of the orthorhombic Y123 grains can be evaluated from the traces of three known planes, (1 1 0), ($\bar{1}$ 1 0) and (0 0 1), on the polished surface. As can be seen in Fig. 1a, there are two twin planes in the Y123 unit cell, (1 1 0) and ($\bar{1}$ 1 0). They are visible on the polished faces as twin traces under optical polarized light. Another known parameter is the trace of the microcracks that was induced by the tetragonal–orthorhombic phase change. The microcracks are developed on the (0 0 1) plane, i.e. the cleavage plane of the Y123. The interplanar angles between the two twin traces and the microcracks can be evaluated and hence the orientation of the polished faces can be approximately determined. As shown in Fig. 1b, for example, the two twin traces on the (0 0 1) plane cross

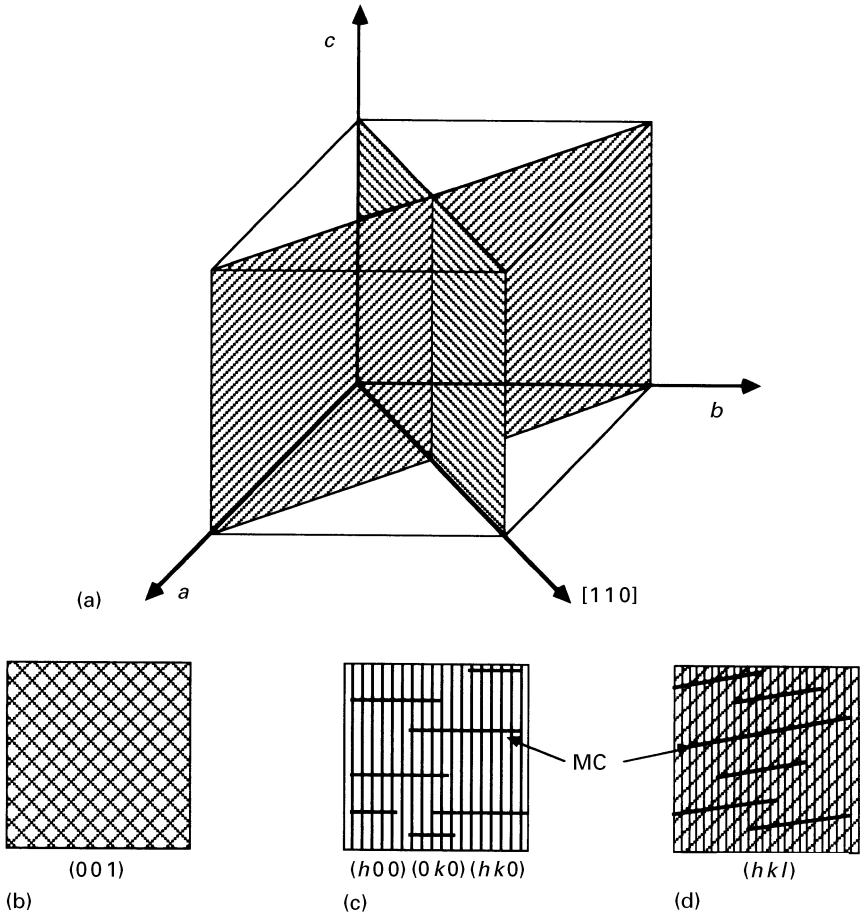

Figure 1 Schematic drawing of (a) {1 1 0} twin planes in the unit cell and (b–d) orientation relationship among two twin traces and microcracks on various crystallographic planes. MC denotes a microcrack. (b) Microcrack not visible, (c) microcracks normal to the twin traces, and (d) microcracks at an angle to the twin traces.

each other with an angle of 90° and no microcracks are visible because they lie on this plane. On the other hand, only one twin trace is visible on planes such as the (h 0 0), (0 k 0) and (h k 0) planes, these planes are parallel to the [0 0 1] direction, while the direction of the microcracks is viewed normal to the twin traces (see Fig. 1c). On the other planes, with the exclusion of the above planes, as shown in Fig. 1d the two twin traces and the microcracks meet each other with an angle of 0–90°. On the basis of the orientation relations, the orientations of the polished surfaces of the melt-textured Y123 domains and the two-dimensional shape of the Y211 patterns on the known (h k l) plane are estimated.

3. Results

3.1. Two-dimensional Y211 patterns within the Y123 domain

The size of the Y123 domains of the melt-textured Y123 samples was dependent on the cooling rate from the peritectic temperature to the Y123 phase region (1010–970 °C in the applied heating cycles): large Y123 domains a few millimetre–centimetre in size were produced at the rate of 1 °C h^{-1} and small domains of a few hundreds of micrometre at 5 °C h^{-1}. In all the melt-textured Y123 samples, it was found that the Y211 particles were trapped with an x-like pattern within the Y123 domains.

On the polished surfaces of the melt-textured Y123 samples, the domain with a plane close to the (h 0 0), (0 k 0), (0 0 l) and (h k 0) were selected for orientation analysis, because the orientation analysis for these planes is easier than other planes. Fig. 2 shows the microstructure of the (0 0 1) plane: (a) the etched microstructure of the Y123 domain, and (b) a polarized micrograph of Fig. 2a. The crystallographic orientation of the polished Y123 surface can be estimated from the orientations of the twin traces of Fig. 2b. The small angle of the crossing twin traces is 88°, which indicates that this plane is very close to the (0 0 1) plane of Y123 (the crossing angle of this plane is 90°). As can be seen in Fig. 2a, an x-type Y211 pattern is observed, with square tracks in the centre of the Y211 pattern. The four diagonal parts of the Y211 tracks are parallel to the ⟨1 1 0⟩ twin traces. Such a Y211 pattern is a typical one that is viewed on the a–b plane of the Y123 and has already been reported in previous works [10–12].

In order to examine the variation of Y211 pattern with domain thickness, the observed Y123 domains including the Y211 pattern were ground and polished repeatedly to a thickness of about 30–50 μm until it disappeared. A typical example of the result is shown in Fig. 3. As can be seen in Fig. 3a, the microcracks that are formed on the (0 0 1) plane (marked C), are almost perpendicular to the ⟨1 1 0⟩ twin traces, but are parallel to the longer side of the Y123 domain. The smaller angle between the two twin traces is less than 5°, which indicates that this polished surface is close to the (h k 0) type plane that is normal to the [0 0 1] direction of Y123. In this Y123 domain, an x-type Y211 pattern is also observed, with rectangular Y211

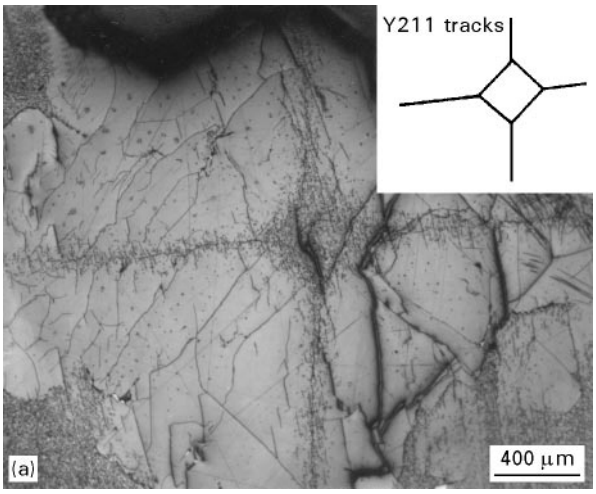

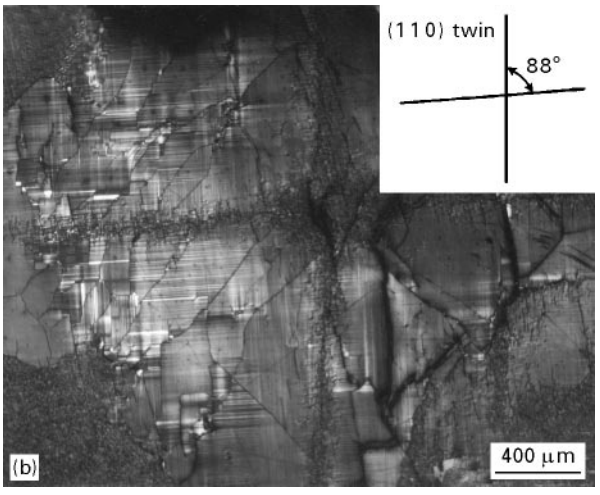

Figure 2 Microstructure of the polished surface close to the (0 0 1) plane of the melt-textured Y123 sample: (a) the x-type Y211 pattern, and (b) the twin traces. Note the directions of the diagonal Y211 tracks are the same as those of the twin traces.

tracks in the centre part. Two sides of the rectangular Y211 are parallel to the direction of the microcracks and the other two sides are normal. This indicates that two sides are parallel to [1 0 0] and [0 1 0], while the other two sides are parallel to the [0 0 1] direction of Y123. On the other hand, the four diagonal Y211 tracks meet at the corners of the Y123 domain. This Y211 pattern is quite similar to that observed on the (0 0 1) plane of Fig. 2. As can be seen in the series of Y211 patterns shown in Fig. 3a–d, the x-type pattern is always observed within the Y123 domains regardless of the sample thickness. There is no remarkable change in Y211 pattern except the change in size of the rectangular Y211 track that is located at the centre. From the series of two-dimensional Y211 patterns one can easily understand the three-dimensional Y211 pattern. The Y211 pattern consists of Y211 tracks that lie on the surfaces of the three sets of {1 1 0} type diagonal planes that stretch towards the corners of the Y123 domain. Not illustrated here, we examined various Y211 patterns that were two-dimensionally viewed on the polished Y123 surfaces and the results were used for inferring the three-dimensional Y211 pattern.

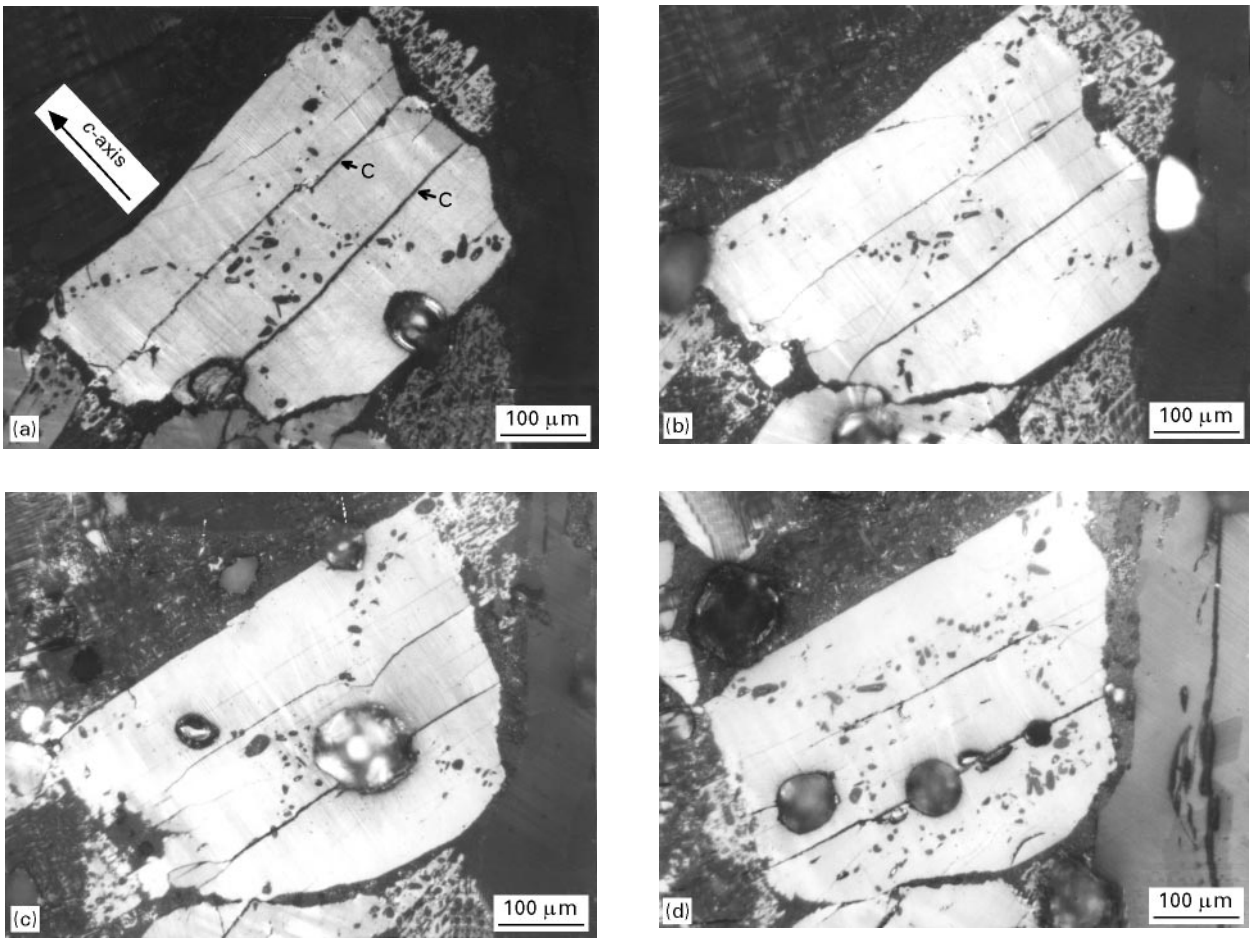

Figure 3 Variation of the Y211 pattern on the ($h\,k\,0$) type polished surface with domain thickness. Note that an *x*-type Y211 pattern is always observed in the Y123 domain regardless of the thickness. C denotes a microcrack.

3.2. Three-dimensional shape of the Y211 pattern

From the microstructural investigations, it can be realized that there are several common features of the Y211 pattern:

1. one *x*-type Y211 pattern is included within the Y123 domain,

2. the diagonal Y211 tracks meet with the corners of the Y123 domain and

3. one set of diagonal Y211 tracks is in the same orientation as the $\langle 1\,1\,0 \rangle$ twin direction and

On the basis of this information, the three-dimensional shape of the Y211 pattern was drawn and the results are shown in Fig. 4a–f. Although the crystal structure of Y123 is orthorhombic, the crystal unit is simplified as a cubic because the *a*-axis (lattice constant: 0.382 31 nm) is similar to the *b*-axis (0.388 64 nm) in length and the *c*-axis (1.168 07 nm) is almost three times as long as the *a*- or the *b*-axis [21]. As already observed in Fig. 2, the two diagonal Y211 tracks are parallel to the $\langle 1\,1\,0 \rangle$ twin traces of Y123 on the plane close to the (0 0 1) plane. This indicates that the Y211 tracks lie on (1 1 0) and ($\bar{1}$ 1 0) planes (see Fig. 4b). As observed in the Y211 pattern series of Fig. 3a–d, two sets of diagonal planes, making an angle of about 45° with the microcracks, lie on the *a*–*b* plane of the Y123 domain. The two sets of diagonal planes correspond with the (0 1 1)/(0 $\bar{1}$ 1) and (1 0 1)/(1 0 $\bar{1}$) planes.

In order to confirm the three-dimensional nature of the Y211 pattern, the drawn Y211 pattern was cut along various crystallographic directions of the Y123 and the traces of the Y211 tracks that imaged on the sectioned surfaces were examined. The imaged Y211 traces are compared with the real Y211 patterns that were observed in the microstructures. As can be seen in Fig. 5a, if the sectioned face of the Y123 domain is normal to the *a*–*b*, *a*–*c*, or *b*–*c* plane, the typical *x*-type Y211 pattern including rectangular Y211 tracks at the centre is viewed on the planes. The corresponding example of the Y211 pattern, which was observed in the melt-textured Y123, is shown in Fig. 5d. The imaged Y211 pattern is consistent with the observed Y211 pattern. On the other hand, if the corner of the Y123 domain is cut along a direction neither normal nor parallel to the *c*-axis, the triangular Y123 surface is viewed (see Fig. 5b). On this plane, the three corners and any point in the interior of the triangular Y123 domain are connected by the three linear Y211 tracks. A microstructural example of the Y211 tracks is also illustrated in Fig. 5e. Another example of the trace of the Y211 tracks is shown in Fig. 5c. The twig-like Y211 tracks are imaged on this plane. The corresponding Y211 pattern is shown in Fig. 5f, in which the two diagonal tracks of the Y211 pattern are parallel to the two twin traces.

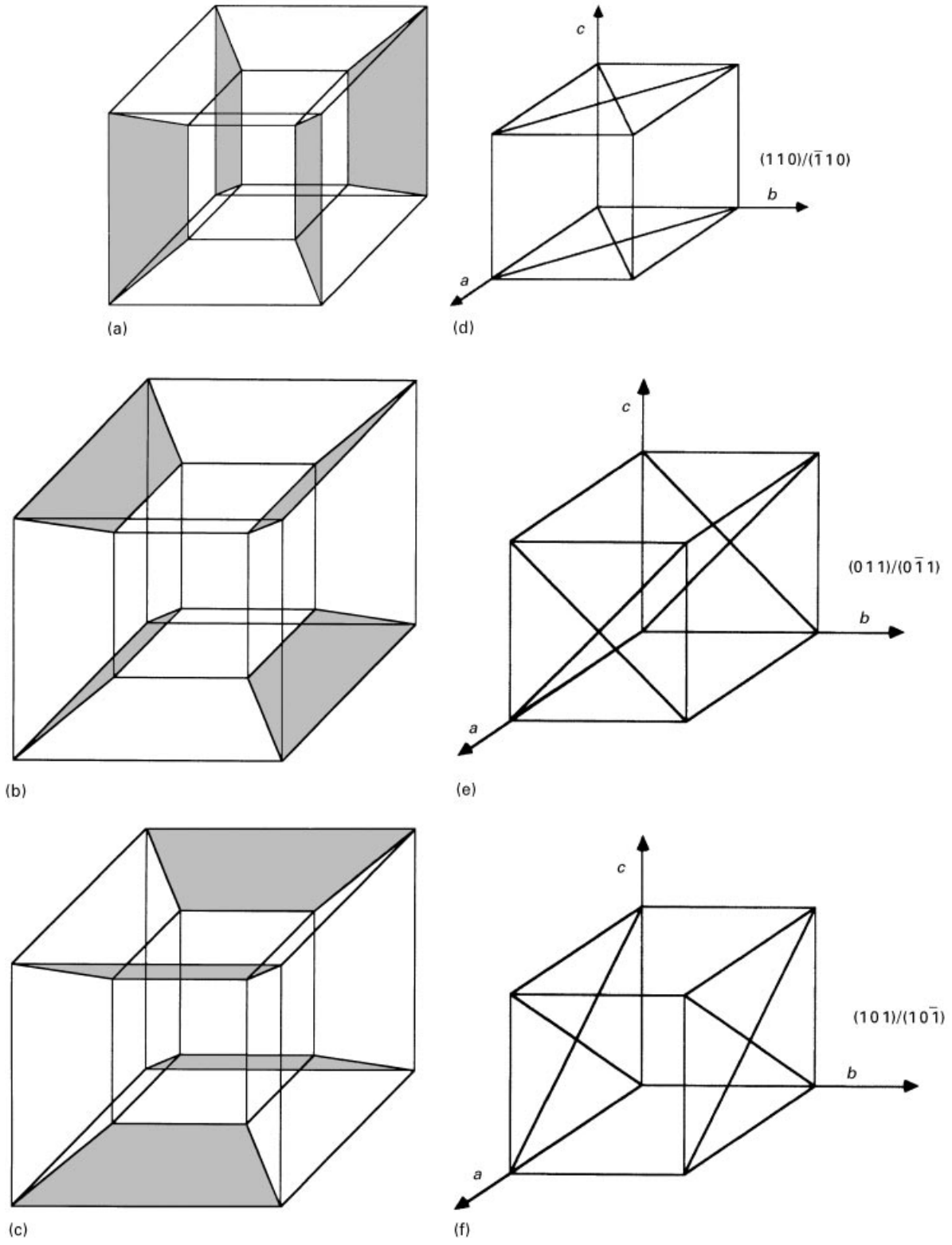

Figure 4 The three-dimensional shape of the Y211 pattern. The dark areas of Fig. 4a–c correspond to the planes on which the Y211 tracks lie. The diagonal Y211 tracks include (1 1 0), ($\bar{1}$ 1 0), (0 1 1), (0 $\bar{1}$ 1), (1 0 1) and (1 0 $\bar{1}$) planes. Fig. 4d–f shows the crystallographic planes of the Y211 tracks in the unit cell.

4. Discussion

4.1. Consideration of the interfacial energy of the Y123

In our previous work [12] and other work [15], the trapping behaviour of Y211 and other impurity particles ($BaCeO_3$ and $BaSnO_3$) ahead of the advancing Y123–liquid interface is described by the UCJ theory [16]. The equilibrium condition of Y211 particle interaction at the advancing Y123–liquid interface is given by ($\sigma_{PS} = \sigma_{PL} + \sigma_{SL}$), where σ_{PS}, σ_{PL} and σ_{SL} are the particle (Y211)–solid (Y123), the particle–liquid and the solid–liquid interfacial free energies, respectively. When σ_{PS} is greater than the sum of σ_{PL} and σ_{SL}, the particle is pushed from the interface towards the liquid

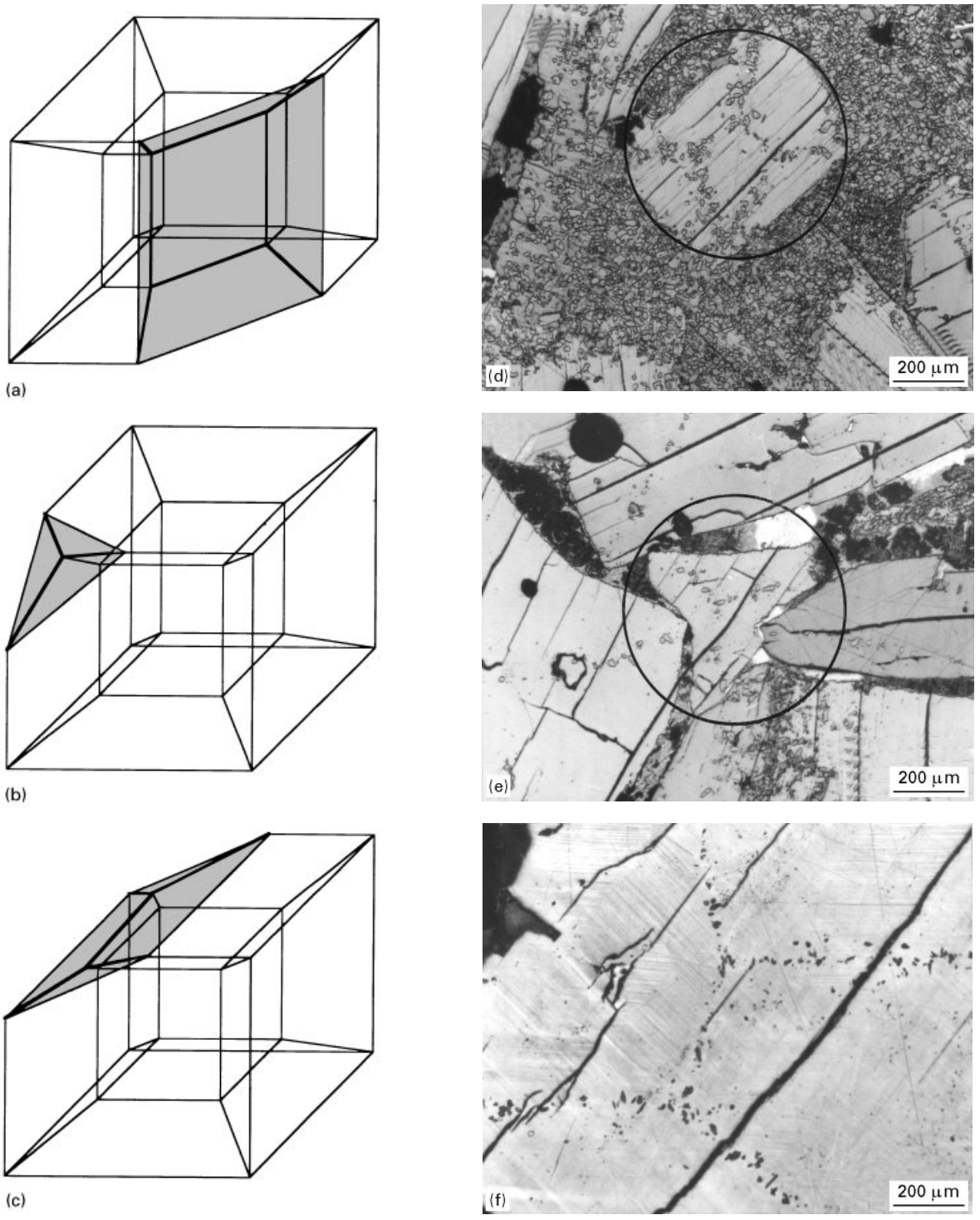

Figure 5 The imaged traces of the Y211 pattern on various sectioned planes (a–c) and the corresponding examples that were observed in the microstructure of melt-textured Y123 samples (d–f).

phase by rapid diffusion of the liquid to the growing solid phase behind the particle. In contrast, when σ_{PS} is less than the sum of σ_{PL} and σ_{SL}, the particle is trapped within the growing solid (Y123). The interfacial energy relations describe well only the condition where Y211 will be pushed out of the advancing Y123–liquid interface or trapped within the Y123 domain. However, this theory cannot explain the formation of the Y211 pattern completely.

UCJ's theory does not consider the difference in interfacial energy among the advancing solid planes. If there is no difference in interfacial energy among the growing planes (this corresponds to isotropic growth), the growth velocity of Y123 is the same at all the interfaces and thus the probability of Y211 trapping will be the same at all the Y123–liquid interfaces. Consequently, the Y211 particles will be trapped randomly within Y123. In this case, the Y211 trapping

behaviour is mainly dependent on the shape and size of Y211. In contrast, if there is a large difference in interfacial energy among the growing planes of Y123, the growth velocity of the Y123 planes varies with the interfacial energy term and it thus leads to the anisotropic growth mode: the specific crystallographic plane of Y123 will grow faster than the other planes. In a solid crystal showing an anisotropic growth mode like the Y123 domain, in general, there is a large difference in the interfacial energy of the growing $(h\,k\,l)$ planes. As shown in Fig. 6, i.e. a schematic for growth of the a–b plane in the liquid phase, the interfacial energy, $\sigma_{1\,1\,0}$, of the (1 1 0) plane (the corner of the domain) is quite different from the interfacial energy, $\sigma_{1\,0\,0}/\sigma_{0\,1\,0}$, of the (1 0 0)/(0 1 0) plane (the planar fronts). The criteria on the Y211 trapping among the planes are different: for the $(h\,k\,l)$ planes, $\Delta\sigma_{(h\,k\,l)} = \sigma_{PS(h\,k\,l)} - (\sigma_{PL} + \sigma_{S(h\,k\,l)L})$ and the value of $\Delta\sigma_{(1\,1\,0)}$ is not the same as that of $\Delta\sigma_{(1\,0\,0)}$ or $\Delta\sigma_{(0\,1\,0)}$. This leads to a difference in velocity of the growing planes. Owing to the fact that trapping of the Y211 is a function of the growth velocity of Y123, at the slowly advancing Y123–liquid interfaces, the Y211 particles will be easily pushed towards the liquid phase while at the fast advancing interfaces Y211 will be trapped. This is partly attributed to the different pushing-out behaviours of the Y211 particles ahead of the advancing Y123 planes.

A typical example of the suggested Y211 trapping mode is shown in Fig. 7. The microstructure shows the region where the two growing Y123 domains in the liquid plus Y211 and the trapping of the Y211 particles are in progress. Most of the growing fronts are planar but the corners of the two growing Y123 domains are open, where many Y211 particles are being trapped along the specific crystallographic directions of the Y123 domains. This result strongly implies that the formation of the Y211 tracks resulted from anisotropic growth mode of the Y123 domain due to differences in interfacial energy among the growing planes.

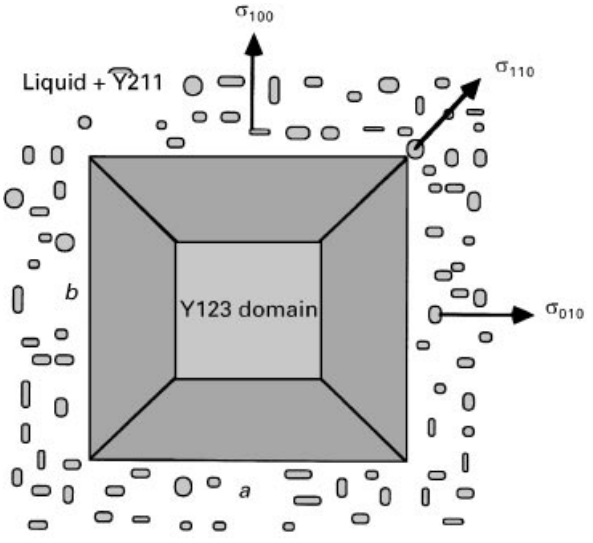

Figure 6 Schematic of the anisotropic growth mode of Y123 in the liquid phase due to the difference in interfacial energy among the growing planes. $\sigma_{1\,0\,0}$, $\sigma_{0\,1\,0}$ and $\sigma_{1\,1\,0}$ denote the interfacial energy of the (1 0 0), (0 1 0) and (1 1 0) planes of the Y123 domain, respectively.

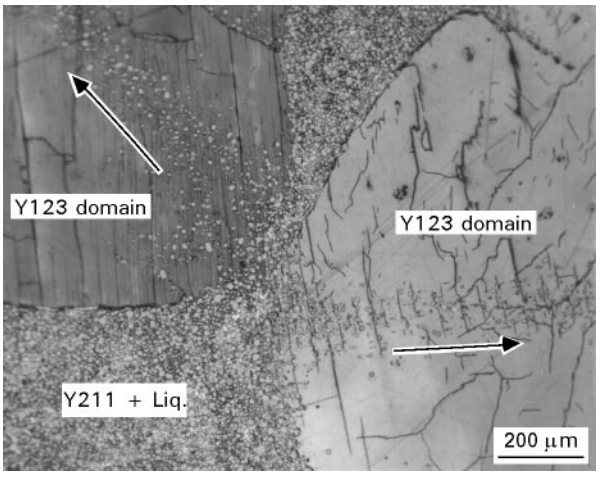

Figure 7 The growth of the two Y123 domains in the liquid plus Y211 and the trapping of the Y211 along the specific crystallographic direction of Y123.

4.2. Growth mode of the Y123 domain

In addition to consideration of the interfacial energy of the growing Y123 planes, the growth shape of the Y123 domain may affect the formation of the Y211 pattern. In order to understand the growth shape of the Y123 domains, the surfaces of the melt-textured Y123 samples are investigated and SEM micrographs are shown in Fig. 8a–c. Fig. 8a shows the Y123 domain that was grown in the vicinity of a large pore. It can be seen that the Y123 domain consists of a square pyramid with stepped terraces at the top and a tetragonal columnar body. Details of the growth shape of the Y123 domain will be reported in another work [22]. Such a growth mode corresponds to the (0 0 1) plane of the Y123. A noticeable fact is that on the top surface the four diagonal arms are stretched along the ⟨1 1 0⟩ directions, which are the same directions as those of the diagonal Y211 tracks of the x-type Y211 pattern observed in Figs 2 and 3. The x-type diagonal arms are always observed in all the surface micrographs of the Y123 domains.

Fig. 8b shows another example of the surface morphology of the Y123 domain, which clearly reveals the details of the Y123 growth mode. It should be pointed out that the Y123 domain is not a simple stack of Y123 plates, but a gathering, in part, of several stacks of cellular Y123. The cellular Y123 platelets appear to be independently grown in the four regions that are separated by the diagonals. In the regions marked A and B, the Y123 platelets seem to grow in the [0 0 1] or [0 1 0] direction, with a two-dimensional cellular or dendritic mode. Meanwhile, the large cellular Y123 grains in the region marked C grow normal to the Y123 platelets of regions A and B. The Y123 platelets

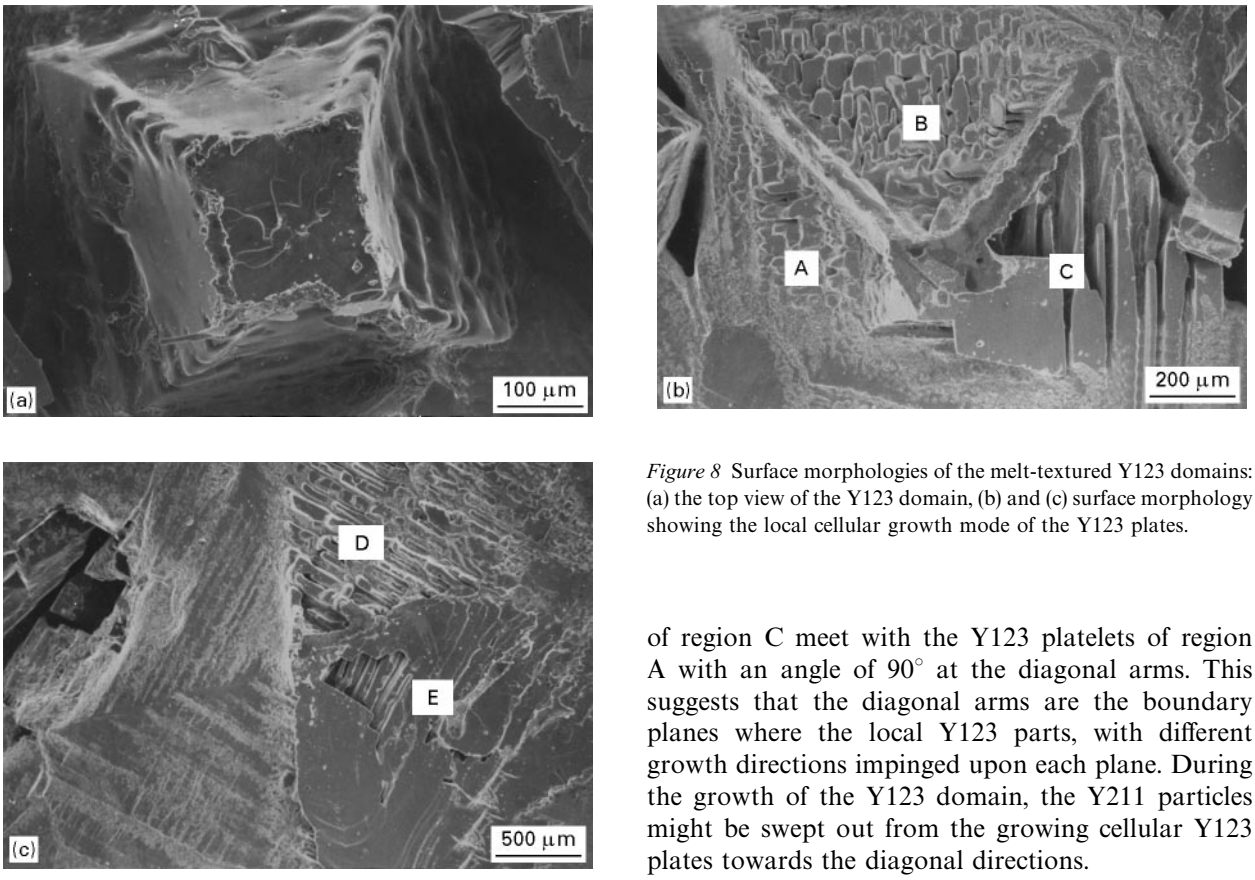

Figure 8 Surface morphologies of the melt-textured Y123 domains: (a) the top view of the Y123 domain, (b) and (c) surface morphology showing the local cellular growth mode of the Y123 plates.

of region C meet with the Y123 platelets of region A with an angle of 90° at the diagonal arms. This suggests that the diagonal arms are the boundary planes where the local Y123 parts, with different growth directions impinged upon each plane. During the growth of the Y123 domain, the Y211 particles might be swept out from the growing cellular Y123 plates towards the diagonal directions.

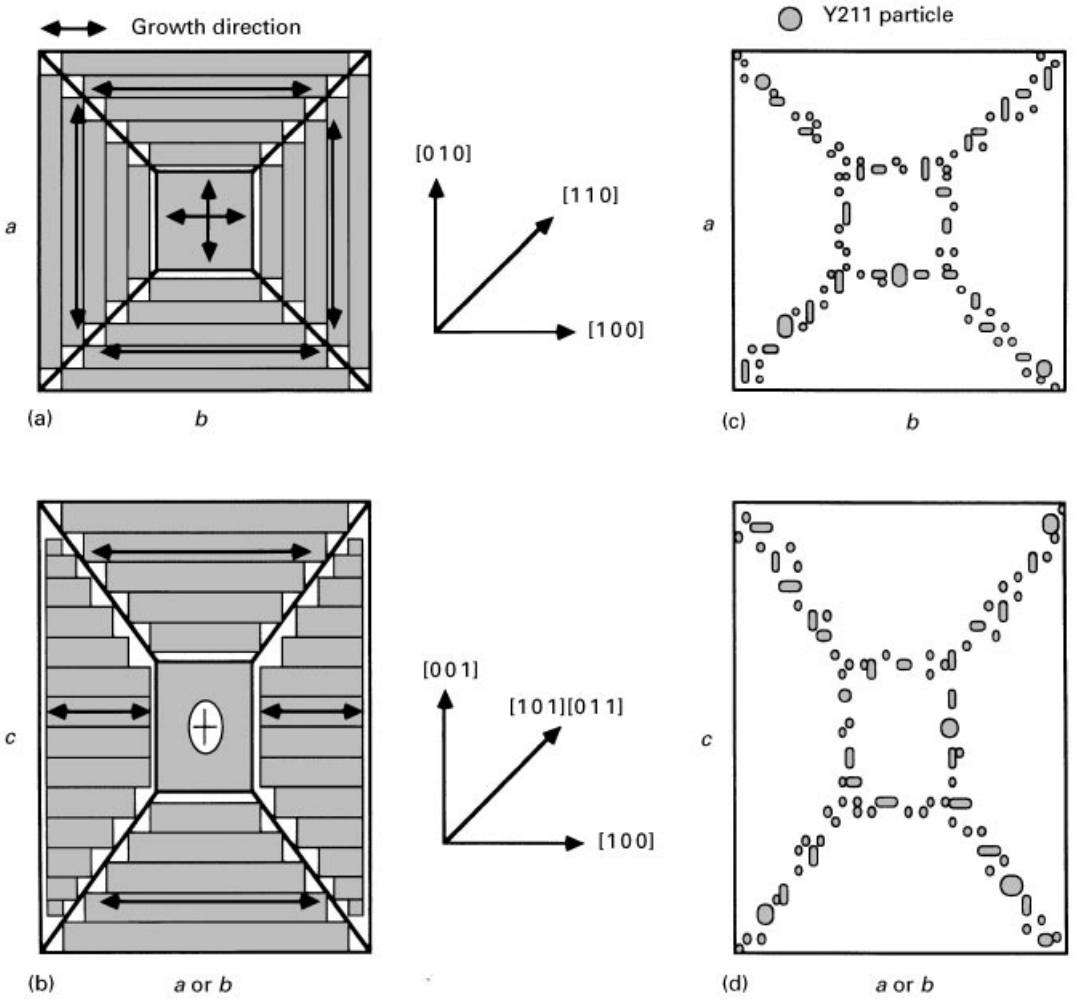

Figure 9 Schematic illustration of the growth mode of the Y123 domain and the Y211 pattern on the *a–b* and *a–c* planes.

Fig. 8c shows a surface morphology that is similar to the Y123 domain that is much deviated from the [0 0 1] direction. Also, cellular growth mode of the Y123 plates is observed, which is divided into four parts by the *x*-type diagonals. The Y123 plates between neighbouring parts are normal in growth direction (see the cellular Y123 plates of region D and in the hole of region E). The complicated growth mode of the Y123 domain is also responsible for the formation of the Y211 pattern.

Our microstructural results show that the melt-textured Y123 domain is a single crystalline body containing trapped Y211 and some microcracks, but the local parts of the Y123 domain were independently grown. Fig. 9 shows a schematic illustration of the growth mode of the Y123 domain that is inferred from the observed microstructures and the Y211 pattern: (a) is for the *a*–*b* plane, and (b) is for the *a*–*c* or the *b*–*c* plane, respectively. As already observed in Fig. 8, the rectangle or square region of Y123 was observed in the centre of the Y123 domain. This is consistent with the rectangular Y211 tracks in the centre of the *x*-type Y211 pattern. The Y123 rectangular region is considered to be the initially grown part of the Y123 domain, and the outer cellular Y123 grains as the region that was formed later. Although the exact growth mechanism of the Y123 domain is not clear, at the initial growth stage the Y123 domain is grown with planar fronts and then the growth mode changes to cellular or dendritic growth when it exceeds the critical size. Probably, it can be related to the degree of undercooling, (ΔT), from the peritectic temperature and the cooling rate to the lower temperature (cooling of $1\,^{\circ}C^{-1}\,h^{-1}$ from 1010 to 970 °C in this experiment). Further systematic work is needed to determine the influence of ΔT and cooling rate on the Y123 shape and the formation of the Y211 pattern.

5. Conclusions

The crystallographic orientations of the Y211 pattern, which was formed within the melt-textured Y123 domain, were determined from the orientation relationship among the Y211 tracks, $\langle 1\,1\,0\rangle$ twin traces and microcracks. From the analysed orientations of the Y211 tracks in the two-dimensional Y211 patterns, the three-dimensional shape of the Y211 pattern was inferred as follows:

1. one *x*-type Y211 pattern is included within one Y123 domain,

2. the diagonal Y211 tracks meet with the corners of the Y123 domain, and

The Y211 tracks lie on (1 1 0), ($\bar{1}$ 1 0), (0 1 1), (0 $\bar{1}$ 1), (1 0 1) and (1 0 $\bar{1}$) planes of the Y123 domain. The Y211 pattern seems to be formed as a result of anisotropic grain growth of the Y123 domain that pushes out the Y211 from the advancing Y123–liquid interface towards the specific orientations of the Y123, as well as the growth shape of the Y123 domain. The planes on which the Y211 tracks lie correspond to the boundary where the local parts of the Y123 domain are impinged upon each other.

Acknowledgements

The authors wish to thank the Ministry of Science and Technology (MOST), Korea for financial support for this work.

References

1. S. JIN, R. SHERWOOD, E. M. GYORGY, T. H. TIEFEL, R. B. VAN DOVER, S. NAKAHARA, L. F. SCHNEEMEYER, R. FASTNACHT and M. E. DAVIS, *Appl. Phys. Lett.* **54** (1989) 584.
2. M. MURAKAMI, M. MORITA, K. DOI and K. MIYAMOTO, *Jpn. J. Appl. Phys.* **28** (1989) 1189.
3. M. MORITA, K. MIYAMOTO, K. DOI, M. MURAKAMI, K. SAWANO and S. MARSUDA, *Physica C* **172** (1990) 383.
4. K. SALAMA, V. SELVAMANICKAM, L. GAO and K. SUN, *Appl. Phys. Lett.* **54** (1989) 2352.
5. L. ZHOU, P. ZHANG, P. JI, K. WANG, J. WANG and X. WU, *Supercond. Sci. Technol.* **3** (1990) 490.
6. P. J. MACGINN, W. CHEN, N. ZHOU, M. LANAGAN and U. BALACHANDRAN, *Appl. Phys. Lett.* **57** (1990) 1455.
7. C.-J. KIM, H.-W. PARK, K.-B. KIM and G.-W. HONG, *Supercond. Sci. Technol.* **8** (1995) 652.
8. C.-J. KIM, K.-B. KIM and G.-W. HONG, *Mater. Lett.* **20** (1994) 283.
9. C.-J. KIM, K.-B. KIM, D.-Y. WON and G.-W. HONG, *Physica C* **228** (1994) 351.
10. C. VARANASI and P. J. MACGINN, *ibid.* **207** (1993) 79.
11. C.-J. KIM, S. H. LAI and P. J. MCGINN, *Mater. Lett.* **19** (1994) 185.
12. C.-J. KIM, K.-B. KIM, G.-W. HONG and H.-Y. LEE, *J. Mater. Res.* **10** (1995) 1605.
13. C.-J. KIM, H.-G. LEE, K.-B. KIM and G.-W. HONG, *ibid.* **10** (1995) 2235.
14. N. VANDEWALLE, M. AUSLOOS, N. MINEUR, R. CLOOTS, G.-W. HONG and C.-J. KIM, *Supercond. Sci. Technol.* **9** (1996) 665.
15. T. IZUMI, Y. NAKAHARA and Y. SHIOHARA, *ibid.* **7** (1992) 1621.
16. D. R. UHLMANN, B. CHALMERS and K. A. JACKSON, *J. Appl. Phys.* **35** (1964) 2986.
17. M. MURAKAMI, S. GOTOH, N. KOSHIZUKA, S. TANAKA, T. MATSUSHITA, S. KAMBE and K. KITAZAWA, *Cryogenics* **30** (1990) 390.
18. H. FUJIMOTO, M. MURAKAMI and N. KOSHIZUKA, *Physica C* **203** (1992) 103.
19. C.-J. KIM, K.-B. KIM and G.-W. HONG, *Supercond. Sci. Technol.* **7** (1994) 812.
20. J. D. VERHOEVEN and E. D. GIBSON, *Appl. Phys. Lett.* **52** (1988) 1190.
21. A. M. T. BELL, *Supercond. Sci. Technol.* **3** (1990) 55.
22. C.-J. KIM, H.-W. PARK, K.-B. KIM and G.-W. HONG, *J. Cryst. Growth* **156** (1995) 398.

Received 3 October 1995
and accepted 10 February 1997